World Conference on Timber Engineering Oslo 2023

DESIGN OF ASYMMETRIC FRICTION CONNECTION FOR SESIMIC RETROFITTING OF RC FRAMES WITH CROSS-LAMINATED TIMBER PANELS

Angelo Aloisio[1,2], Francesco Boggian[1], Roberto Tomasi[2]

ABSTRACT: This paper proposes a probabilistic model for predicting the friction coefficient of asymmetric friction connections to be used for the seismic retrofitting of reinforced concrete buildings using Cross-Laminated Timber (CLT) panels. The model has been calibrated on the experimental force-displacement curves of the AFC samples, tested at the Norwegian University of Life Sciences (Norway), within the e-SAFE research project.

KEYWORDS: Cross-Laminated Timber; Passive Dampers; Friction dampers; Seismic retrofitting; Probabilistic models.

1 INTRODUCTION

Among hysteretic devices, friction dampers have been gaining more attention in the last few years. These dampers dissipate seismic energy by mechanical damping through sliding friction with the primary braking rather than breaking principle [1]. There is a wide range of applications of friction dampers, from civil to mechanical and avionic engineering [2]. However, there are still a few attempts to use friction dampers for seismic retrofitting civil structures. Venuti 1976 [3] and Pall et al. in 1980 [4] were the first to add friction devices as additional damping sources in civil structures. The Limited Slip Bolt (LSB), evolved to the Pall Frictional Damper (PFD), exhibited stable, almost rectangular hysteresis cycles [5], [6]. PFD is conceived for X- and K-bracings. Its worldwide success has confirmed the merits of the PFD. Multiple applications and research papers are proving the value and efficiency of the PFD [7]–[10]. The main drawbacks of PFD are the relatively low capacity (less than 10 kips), the need for high precision work for its manufacture, and specialized training for the installation process [11], [12].
In 1989 Fitzgerald et al. [13] devised a friction connection called the Slotted Bolted Connection (SBC), characterized by a more straightforward design than the PFD. The proposed SBC worked by sliding channel bracing plate over a gusset plate interconnected by high strength bolts with washers (Belleville spring) for adjusting the bolt tension.
There are two main classes of SBC: the Symmetric and Asymmetric friction connection [14], [15]. Symmetric Friction Connection (SFC) is a type of SBC that consists of the main plate (with slotted holes), two brass shims, two outer plates, and high strength bolts.
Initially proposed by Clifton [16], Asymmetric Friction Connection (AFC) is another type of SBC [17], [18]. AFCs consist of steel plates and shim layers clamped by the pre-tensioned bolts.
AFC is a crucial component of Sliding Hinge Joints (a low damage beam-to-column connection for the Moment Resisting Frame). AFCs installed in SHJ consist of shims, cleat, cap plate, high strength bolts, and bottom flange of the beam. The friction originates from the sliding between (i) beam bottom flange and upper shim and (ii) cleat and lower shim [16]. Initial developments of AFC were based on brass shims [19]. Subsequent studies by Mackinven [20] extended the application to mild steel and aluminium shims. The AFC is simple to build, cost-effective, and capable of dissipating energy under seismic excitation.
However, the AFC hysteretic stability highly depends on the mutual hardness between the steel and shim layers. In addition, the stability of the hysteretic performance is affected by the interaction between abrasive and adhesive wear and friction phenomena. There are several examples of application of AFC connections in real buildings, see [21], [22]. A few scholars [23]–[27] attempted to verify the consequences of wear and friction on AFC in the past years. They found that a stable cyclic behaviour can be achieved if there is a significant difference in the mutual hardness of the siding surfaces, i.e. shim layer and steel plates. The similarity in sliding surfaces' hardness causes a significant instability of the hysteresis loop mainly due to the large amount of work-hardened wear particles produced during the sliding mechanism. These particles abrade the sliding surfaces in an irregular pattern, thus exhibiting a wear abrasive mechanism defined by Grigorian and Popov [19] and Khoo et al. [18]. The stability of the hysteresis curve, in the case of non-lubricated sliding surfaces, depends on the initial wear of the shim or steel plates. For instance, in the case of the shim layer being less hard than the plates, the initial wear increases the roughness of the shim layer. The wear particles generated in this process create lubrication that

[1] University of L'Aquila, Italy
[2] Faculty of Science and Technology, Norwegian University of Life Sciences, Oslo, Norway

https://doi.org/10.52202/069179-0411

stabilizes the friction coefficient. Therefore, the wear particles generated in the initial phase are crucial to achieving a stable performance of the AFC.
Aluminium shims are among the materials that exhibit the best performance, with the lowest and more stable friction coefficient. Currently the shims to be used in AFC are recommended to be abrasion-resistant, like (high hardness) steel [21]. Nonetheless, AFCs with high hardness cleat and high hardness shims do not provide specific benefit on the seismic performance [28].
There are different typologies of AFCs. The most used and studied is the Sliding Hinge Joint (SHJ). The SHJ is a flexural connection designed to use at the beams' ends in steel moment-resisting frames. It is an AFC where energy is dissipated through sliding in slotted bolted connections in the beam bottom flange [29]. The initial application of friction connections to low-damage moment-resisting joints has been recently extended to pinching-free connections for timber structures [30]. Pinching represents one of the significant weaknesses in timber structures since it is associated with considerable degradation after repeated cycles [31], [32]. Loo et al. [33] investigated the possibility of using SFC instead of hold-down for restraining timber shear walls against uplift, to cap the force transmitted to the wall, and reduce inelastic damage. The subsequent experimental campaigns presented in [15] established the effectiveness of SFC on reducing the degradation and pinching phenomena typical of timber connections. The following studies presented in [34] pointed to a displacement-based design method for multistorey CLT buildings with friction connections. Next to the findings by Loo et al., [35] studied the response of SFC connected to a CLT panel. Zamani and Quenneville proposed a resilient slip friction connection (RSF) as a hold-down connector for CLT panels [36]. So far, no AFC was used as a connection system for CLT panels except for the attempts by Boggian et al. [37]–[39]. Boggian et al. tested AFCs for a hybrid structural system, the e-CLT technology.

2 MECHANICAL RESPONSE OF THE E-CLT

Fig.1 shows the representation of the e-CLT system applied to a building. CLT panels are attached to the beams of each floor with a couple of friction connections (AFC), which can act as rigid connections or slide according to the entity of the horizontal force acting on the building. The basic functioning principle of the AFC is illustrated in Fig.2. When the applied force is below a certain threshold the AFC doesn't activate and stays in the *stick phase*, thus the total resisting force at the i-th story (f_t) is the summation of the resisting forces of the CLT panel (f_{clt}) and the RC frame (f_{rc}). If the reaction of the CLT panel exceeds the slip force (f_s), the AFC activates and transitions to the *slip phase*, and thus the total resisting force is the summation of the resisting force of the RC frame and the slip force of the AFC.

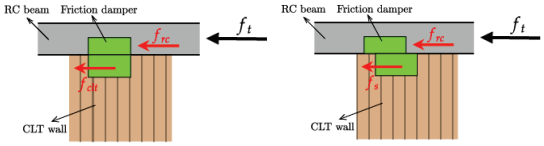

(a) (b)

***Figure 1**: Illustration of the contributions of forces: (a) before the AFC activation and (b) after the AFC activation.*

The e-CLT unit behaves like a parallel system, whose governing equations are:

$$f_t = f_{\mathrm{rc}} + f_{\mathrm{clt}} \quad \text{if} \quad |f_{\mathrm{clt}}| \le |f_s| \tag{1}$$

$$f_t = f_{\mathrm{rc}} + f_s \quad \text{if} \quad |f_{\mathrm{clt}}| > |f_s| \tag{2}$$

The conditional statement on the exceedance of the slip force drives the transition between the two stick and slip phases of the response.

3 EXPERIMENTAL TESTS

The data used in this paper descend from an experimental campaign on AFC specimen at component level. The full campaign is described in [40], and this section will give a synthetic overview of the activity. The specimen, called HYB, is shown in Fig.2, and is composed by an anchor profile (fixed rigidly to the beam of each floor/testing machine during the experiments) and a free profile, which is connected both to the CLT panel, with a screw connection, and to the anchor profile, with two preloaded bolts which allow for sliding in an elongated hole. Both profiles are made of cold bent steel and are 8mm thick. The friction connection is completed by a cap plate and 2 aluminium shim layers to improve the stability of the friction behaviour, which are 2mm thick.

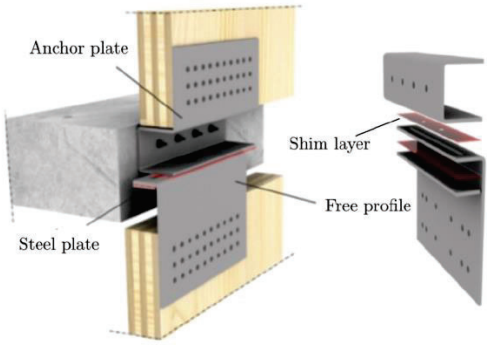

***Figure 2**: Illustration of the tested specimen.*

3.1 OVERVIEW OF THE TESTS

A total of 20 tests was carried out, on 5 different specimens. Every specimen was tested more times and in some cases with different preload forces. The main setup is shown in Fig. 3. The anchor plate is attached to the cross head of the testing machine, which moves up and down, simulating the horizontal movement of a beam subjected to seismic forces. The free profile is connected to a 100mm thick CLT panel with 33 10x80 screws, and to the anchor profile with 2 M16 bolts. The tests were carried out in displacement control method, with a speed of

https://doi.org/10.52202/069179-0411

2mm/s and the following cyclic protocol: 1x5-10mm+3x20-40-60-80-100mm. Fig.3 shows a picture of the main setup and a scheme with the indication of the various sensors acquiring data. The thermocouple was placed directly on the steel plate where friction was occurring.

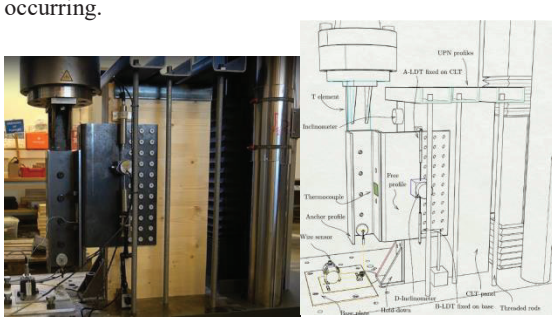

***Figure 3**: Main setup for the testing activity.*

3.2 RESULTS

An extract of the results is shown in Fig.4 for specimen HYB-3. The load displacement graph shows shape that resembles a rectangle, which would be the ideal shape for friction connections hysteresis loops. In this case the shape is not a pure rectangle because it represents the hysteresis of the whole system, which included the deformability of the steel plates and the screw connection. The S-like shape at the branches where the load changes direction is due to the pinching of the timber connection. Full detailed results are presented in [40].

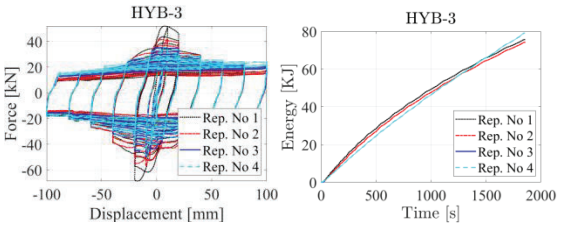

***Figure 4**: Results for specimen HYB-3.*

3.3 ESTIMATE OF THE FRICTION COEFFICIENT

The estimate of the slip force, and thus the friction coefficient, from experimental data is not direct and requires the definition of an approach. This is because the force changes during the tests and the sign changes. The definition of slip force is based on the cumulated dissipated energy, which is a strictly increasing function, as seen in Fig.5. The dissipated hysteretic energy can be defined as follows:

$$E = \sum_{i=0}^{n} E_i = \sum_{i=0}^{n} \left| \frac{F_{i+1}+F_i}{2} \cdot (\delta_{i+1} - \delta_i) \right| \quad (3)$$

where E is the dissipated energy, E_i the dissipated energy at the $i-$th time step, F_i and δ_i are the force and displacement at the same time step, respectively.

The cumulative distance of travel D is the sum of the displacement time steps:

$$D = \sum_{i=0}^{n} |\delta_{i+1} - \delta_i| \quad (4)$$

The slip force is defined as the work per unit of length:

$$F_{\text{slip}} = \frac{E}{D} \quad (5)$$

The experimental friction coefficient μ is finally calculated as

$$\mu = \frac{F_{\text{slip}}}{n_s n_b F_P} \quad (6)$$

where F_{slip} is the slip force calculated in Eq.(5), n_s is the number of shear surfaces equal to 2, n_b is the number of the preloaded bolts equal to 2, and F_P is the preload force. It must be remarked that the above definition of the friction coefficient cannot be entirely interpreted and understood in light of the Amontons laws. Friction in AFC is not just the product of friction between plates mutually sliding. Therefore, the estimated friction coefficient must be considered a system friction coefficient, representing the entire structural performance.

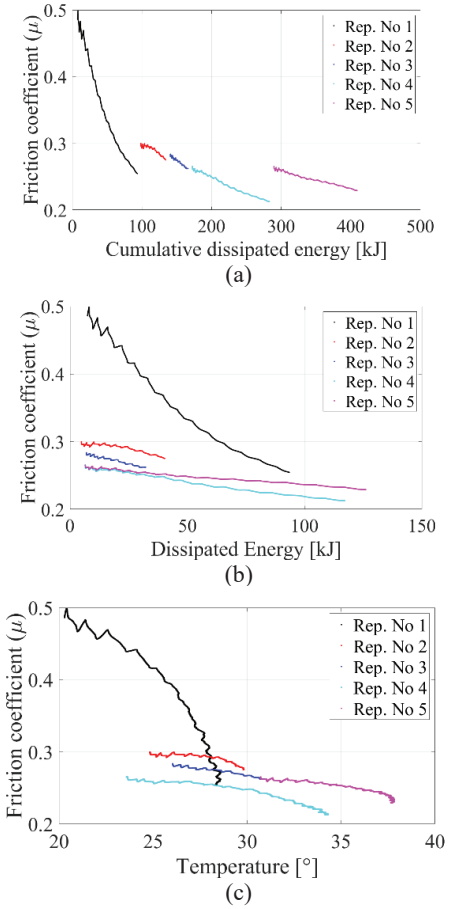

***Figure 5**: Illustration of the contributions of forces: (a) before the AFC activation and (b) after the AFC activation.*

4 PROBABILISTIC FRICTION MODEL

The formulation to predict the friction coefficient can be decoupled into two models. The first model defines the dependence between the value of the friction coefficient estimated at the beginning of each cyclic response μ_0 and its value estimated at the beginning of the first cyclic response from the time of the AFC installation $\hat{\mu}_0$. The second model predicts the value of the friction coefficient μ during each cyclic response starting from the value of

the friction coefficient estimated at the beginning of the response μ_0. The two models will describe two aspects of the friction coefficient evolution. The first will express the dependence of μ on the deformation history. The second will define its evolution during each cyclic response.

Following [40], the model that relates μ_0 to $\hat{\mu}_0$ is formulated as

$$\log(\mu_0) = \log(\hat{\mu}_0) + \gamma_1(\epsilon_p) + \sigma_1\varepsilon \quad (7)$$

where ϵ_p is the dissipated energy accumulated from the past loading tests of the specimen up to the beginning of the cyclic response to be simulated and $\sigma_1\varepsilon$ is the model error, with σ_1 model standard deviation and ε normally distributed random variable. The logarithm is used as variance stabilizing transformation.

The correction term $\gamma_1(\hat{\epsilon}_p)$ is constructed as a polynomial function of ϵ_p. The relevant terms in the polynomial function are selected using the procedure followed in [40]. The selection process (i.e., the removal of explanatory functions from the initial model) stops after a cumulative increase of the model standard deviation greater than 5% that would lead to an excessive loss of accuracy. Although the number of terms in a probabilistic model is often selected in order to balance accuracy and ease of use, in this case, given the limited amount of data available for the calibration, the number of terms is limited to avoid possible over-fitting of the data.The model for μ is formally similar and can be written as

$$\log(\mu) = \log(\mu_0) + \gamma_2(\epsilon_p, \epsilon_d, \hat{\mu}_0) + \sigma_2\varepsilon \quad (8)$$

with ϵ_d dissipated energy estimated from the beginning of the current load test, without the contributions related to the past deformation history. Among the explanatory functions considered for γ_2 there are $\hat{\mu}_0$ and powers of e_p and e_d up to the fourth order. Increasing the order of the powers of e_p and e_d above the fourth is avoided because it would lead to a limited increase in accuracy but would also result in an impractical and less manageable model. The models resulting from the selection processes read

$$\log(\mu_0) = \log(\hat{\mu}_0) + \theta_1{\epsilon_p}^{\frac{1}{2}} + \sigma_1\varepsilon \quad (9)$$

and

$$\log(\mu) = \log(\mu_0) + \theta_2 + \theta_3\hat{\mu}_0 + \theta_4{\epsilon_p}^{\frac{1}{2}} + \theta_5{\epsilon_d}^2 + \theta_6{\epsilon_d}^3 + \sigma_2\varepsilon \quad (10)$$

Both models are calibrated with a Bayesian approach. For all models, the calibration is performed at each stage of the model selection process with the STAN package of the R software that uses a gradient descend method.

Ref provides the statistics of the unknown parameters $\boldsymbol{\Theta} = \{\boldsymbol{\theta}, \boldsymbol{\Sigma}\}$, with $\{\boldsymbol{\theta} = \{\theta_1 \dots \theta_5\}$ and $\boldsymbol{\Sigma} = \{\sigma_1, \sigma_2\}$. The Adjusted R-squared for the two models are Adj-R^2=0.8287 for the model of $\log(\mu_0)$ and Adj-R^2=0.7217 for the model of $\log(\mu)$.

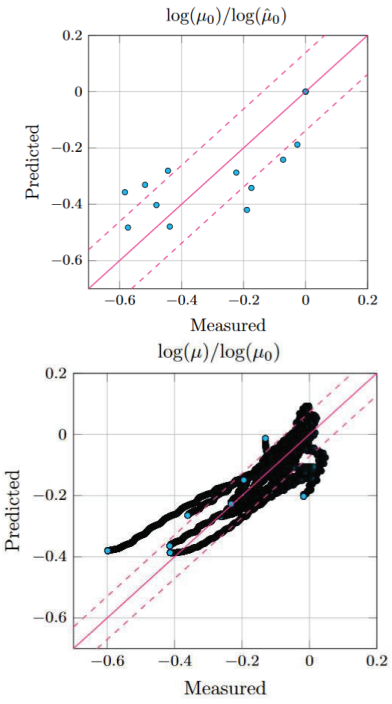

Figure 6: *: Predicted capacity versus measured values of the*

Fig.6 (a) and (b) show the predicted versus measured values of the ratios $\log(\mu_0)/\log(\hat{\mu}_0)$ and $\log(\mu)/\log(\mu_0)$, respectively. The closer the data points are to the 1:1 lines (i.e., the continuous lines in the figure), the more accurate are the predictions. The two figures also show the region within one standard deviation of the median value (i.e., the region between the dashed lines). From Fig. 6(b), it is possible to recognise data from different load tests. The predictions related to some of them exhibit a limited bias that may depends on features that are not captured by the explanatory functions considered in the model selection. A prediction for μ can be obtained combining Eq. (9) and Eq. (10) as

$$\mu = \hat{\mu}_0 e^{\theta_2 + \theta_3\hat{\mu}_0 + (\theta_1+\theta_4){\epsilon_p}^{\frac{1}{2}} + \theta_5{\epsilon_d}^2 + \theta_6{\epsilon_d}^3 + \sigma_t\varepsilon} \quad (11)$$

where $\sigma_t = ({\sigma_1}^2 + {\sigma_2}^2)^{1/2}$. To understand if the temperature can be used as a predictor for the values of μ, the temperature measured during the load test, T, is added into the set of the explanatory functions used to find the correction term for $\log(\mu)$, i.e., $\gamma_2 = \gamma_2(\epsilon_p, \epsilon_d, \hat{\mu}_0, T)$. In this case, the inclusion of T among the explanatory function change the selection process, and T is selected among the significant explanatory functions. The modified model for $\log(\mu)$ has the form

$$\log(\mu) = \log(\mu_0) + \theta_6 + \theta_7{\epsilon_p}^{\frac{1}{2}} + \theta_8\epsilon_p + \theta_9{\epsilon_p}^2 + \theta_{10}{\epsilon_d}^3 + \theta_{11}\epsilon_d + \theta_{12}{\epsilon_d}^4 + \theta_{13}T + \sigma_3\varepsilon \quad (12)$$

https://doi.org/10.52202/069179-0411

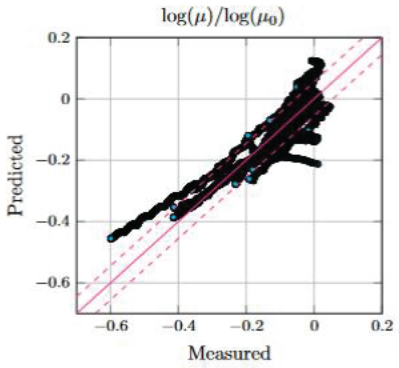

Figure 7: Predicted capacity versus measured values of the friction coefficient.

Fig.7 shows the agreement between the recorded and predicted values of μ, obtained using Eq. (12). The standard deviation of the model error is smaller compared to the model in Eq. (11) and the Adjusted R-squared higher (Adj-R^2=0.8267) . Although the probabilistic friction model dependent on the dissipated energy exhibits a satisfactory performance with an Adj-R^2=0.7217, the inclusion of the temperature as a regressor significantly increases the accuracy of the prediction, leading to an Adj-R^2=0.8267. This increased accuracy does not show the causal link between temperature increment and friction coefficient reduction. Instead, the probabilistic friction model provides evidence of the temperature role without clarifying if it is the cause or the effect of the friction coefficient variation. The experimental results and probabilistic model proved that the proposed structural system based on aluminium shims deserves further improvement to achieve a more stable and reliable hysteretic response.

5 CONCLUSIONS

This research presents the results of quasi-static cyclic tests on Asymmetric Friction Connections (AFC), serving as dissipating devices in the e-CLT system. The e-CLT, proposed under the Horizon 2020 research project e-SAFE, is a seismic retrofitting solution for RC frames based on Cross-Laminated timber (CLT) panels and AFCs. The authors carried out multiple repetitions of the same cyclic load protocol to assess the dependence of the aluminium-steel friction coefficient of the tested AFCs on the temperature, the energy dissipated during the test and that dissipated during the past deformation history of the specimen. The friction coefficient exhibited a significant dependence on both physical quantities. The friction dependence on the dissipated energy during the deformation history might originate from wear phenomena, mainly localized by the bolts, and MPV effects. The mutual sliding between aluminium and steel leads to the abrasive wear of the softer material (aluminium in the current case) and the reduction of the friction coefficient from nearly 0.5 to 0.2 during the first load protocol. Further repetitions of the load protocols on the same specimen also evidenced a dependence on the dissipated energy cumulated during each test. The physical variable possibly responsible for this phenomenon is the increasing temperature during each loading protocol. Following the standard semi-physical approach in hysteresis, the authors developed two probabilistic data-driven friction models calibrated from the experimental data using a Bayesian approach. The data-driven model simulates the evolution of friction without distinguishing between the causes of strength degradation's, like MPV interaction, changes in the properties in the sliding surfaces, and/or prying effects. The first engineering-oriented model depends on the dissipated energy, while the second includes the measured temperature as regressor. The first model exhibits a satisfactory performance with an Adj-R^2=0.7217. However, the presence of temperature as a regressor significantly increases the accuracy of the prediction, leading to an Adj-R^2=0.8267. The higher description capability of the model that includes temperature among the regressors does not show the causal dependence of the friction coefficient reduction on temperature but only the high correlation between the two. Regrettably, the authors do not have multiple tests where the initial temperature of the specimen is varied to rigorously prove the possible dependence of friction on the temperature variation. The first model can predict the friction coefficient in nonlinear analyses of the AFC using a straightforward Coulomb friction model, where the friction coefficient represents an energy-dependent parameter. The authors followed a Bayesian approach for calibrating the coefficients of the friction model, which also provides the complete distributions of the model parameters and allows the update of the model with newly available data.This model can be theoretically extended to different AFCs typologies after proper calibration based on the experimental cyclic response related to multiple load protocols repetitions. Future research efforts, possibly carried out within the Horizon 2020 research grant, will aim to rigorously assess the friction coefficient's dependence on the initial temperature of the specimens.

ACKNOWLEDGEMENT

This paper was carried out in the framework of the Energy and seismic affordable renovation solutions (e-SAFE) project, which has received funding from the European Union's Horizon 2020 research and innovation programme under grant agreement No.893135. Neither the Executive Agency for Small and Medium-sized Enterprises (EASME) nor the European Commission is in any way responsible for any use that may be made of the information it contains.

REFERENCES

[1] A. S. Pall, C. Marsh, and others, Response of friction damped braced frames, *J. Struct. Eng.*, vol. 108, no. 9, pp. 1313–1323, 1982.

[2] L. Pesaresi, M. Stender, V. Ruffini, and C. W. Schwingshackl, DIC measurement of the kinematics of a friction damper for turbine applications, in *Dynamics of Coupled Structures, Volume 4*, Springer, 2017, pp. 93–101.

[3] W. J. Venuti, Energy Absorption of High Strength Bolted Connections, *Test Rep.*, 1976.

[4] A. S. Pall, Energy dissipation devices for aseismic design of buildings, in *Proceedings of a Seminar and Workshop on Base Isolation and Passive Energy Dissipation*, 1986, pp. 223–232.

[5] A. S. Pall and C. Marsh, Friction-damped concrete shearwalls, in *Journal Proceedings*, 1981, vol. 78, no. 3, pp. 187–193.

[6] A. S. Pall, Friction devices for aseismic design of buildings, in *4th Canadian Conference on Earthquake Engineering*, 1983, pp. 475–484.

[7] C. Pasquin, N. Leboeuf, R. T. Pall, and A. Pall, Friction dampers for seismic rehabilitation of Eaton's building, Montreal, in *13th world conference on earthquake engineering*, 2004, pp. 1–2.

[8] R. Chandra, M. Masand, S. K. Nandi, C. P. Tripathi, R. Pall, and A. Pall, Friction-dampers for seismic control of La Gardenia towers south city, Gurgaon, India, 2000.

[9] A. Pall, S. Vezina, P. Proulx, and R. Pall, Friction-dampers for seismic control of Canadian space agency headquarters, *Earthq. Spectra*, vol. 9, no. 3, pp. 547–557, 1993.

[10] B. Wu, H. Li, L. Lin, and M. Shan, Seismic retrofit of a city hall in Northeast China with frictional energy dissipators, *J. Build. Struct.*, vol. 19, no. 5, pp. 28–36, 1998.

[11] B. Wu, J. Zhang, M. S. Williams, and J. Ou, Hysteretic behavior of improved Pall-typed frictional dampers, *Eng. Struct.*, vol. 27, no. 8, pp. 1258–1267, 2005.

[12] A. Filiatrault and S. Cherry, Performance evaluation of friction damped braced steel frames under simulated earthquake loads, *Earthq. spectra*, vol. 3, no. 1, pp. 57–78, 1987.

[13] T. F. Fitzgerald, T. Anagnos, M. Goodson, and T. Zsutty, Slotted bolted connections in aseismic design for concentrically braced connections, *Earthq. spectra*, vol. 5, no. 2, pp. 383–391, 1989.

[14] M. Latour, G. Rizzano, A. Santiago, and L. S. da Silva, Experimental response of a low-yielding, self-centering, rocking column base joint with friction dampers, *Soil Dyn. Earthq. Eng.*, vol. 116, pp. 580–592, 2019.

[15] W. Y. Loo, P. Quenneville, and N. Chouw, A new type of symmetric slip-friction connector, *J. Constr. Steel Res.*, vol. 94, pp. 11–22, 2014, doi: 10.1016/j.jcsr.2013.11.005.

[16] G. C. Clifton, Semi-rigid joints for moment-resisting steel framed seismic-resisting systems, ResearchSpace@ Auckland, Auckland, 2005.

[17] H.-H. Khoo, C. Clifton, G. MacRae, H. Zhou, and S. Ramhormozian, Proposed design models for the asymmetric friction connection, *Earthq. Eng. \& Struct. Dyn.*, vol. 44, no. 8, pp. 1309–1324, 2015.

[18] H.-H. Khoo, C. Clifton, J. Butterworth, G. MacRae, and G. Ferguson, Influence of steel shim hardness on the Sliding Hinge Joint performance, *J. Constr. Steel Res.*, vol. 72, pp. 119–129, 2012.

[19] C. E. Grigorian, Energy dissipation with slotted bolted connections, University of California, Berkeley, 1994.

[20] H. Mackinven, Sliding Hinge Joint for steel moment frames experimental testing, *Unpubl. ENCI493 Proj. Report. Dep. Civ. Eng.*, 2006.

[21] S. Ramhormozian and G. C. Clifton, Optimised Sliding Hinge Joint (OSHJ): Design and Installation Guide for a Low Damage Seismic Resisting System. New Zealand Heavy Engineering Research Association, 2020.

[22] S. Ramhormozian, C. Clifton, and S. Gledhill, The Optimised Sliding Hinge Joint (OSHJ): Overview and First Application to a Project, in *International Conference on the Behaviour of Steel Structures in Seismic Areas*, 2022, pp. 837–843.

[23] G. A. MacRae, G. C. Clifton, H. Mackinven, N. Mago, J. Butterworth, and S. Pampanin, The sliding hinge joint moment connection, *Bull. New Zeal. Soc. Earthq. Eng.*, vol. 43, no. 3, pp. 202–212, 2010.

[24] S. Yeung, H. Zhou, H. Khoo, G. C. Clifton, and G. MacRae, Sliding shear capacities of the Asymmetric Friction Connection, in *2013 NZSEE Conference, April*, 2013, pp. 26–28.

[25] G. W. Rodgers, R. Herve, G. A. MacRae, J. Chanchi Golondrino, and J. G. Chase, Dynamic Friction Coefficient and Performance of Asymmetric Friction Connections, *Structures*, vol. 14, pp. 416–423, 2018, doi: https://doi.org/10.1016/j.istruc.2017.09.003.

[26] J. C. Chanchi Golondrino, G. A. MacRae, J. G. Chase, G. W. Rodgers, and G. C. Clifton, Seismic behaviour of symmetric friction connections for steel buildings, *Eng. Struct.*, vol. 224, p. 111200, 2020, doi: https://doi.org/10.1016/j.engstruct.2020.111200.

[27] A. F. Santos, A. Santiago, M. Latour, and G. Rizzano, Analytical assessment of the friction dampers behaviour under different loading rates, *J. Constr. Steel Res.*, vol. 158, pp. 443–459, 2019.

[28] S. Ramhormozian, G. Clifton, S. Maetzig, D. Cvitanich, and G. MacRae, Influence of the Asymmetric Friction Connection (AFC) ply configuration, surface condition, and material on the AFC sliding behaviour, 2016.

[29] H.-H. Khoo, C. Clifton, J. Butterworth, and G. MacRae, Experimental study of full-scale self-centering sliding hinge joint connections with friction ring springs, *J. Earthq. Eng.*, vol. 17, no. 7, pp. 972–997, 2013.

[30] T. Tannert and C. Loss, Contemporary and Novel Hold-Down Solutions for Mass Timber Shear Walls, *Buildings*, vol. 12, no. 2, p. 202, 2022.

[31] A. Aloisio, A. Contento, R. Alaggio, B. Briseghella, and M. Fragiacomo, Probabilistic assessment of a Light-Timber Frame shear wall with variable pinching under repeated earthquakes, *J. Struct. Eng.*, vol. In press, 2022.

[32] A. Aloisio, M. Pelliciari, A. V. Bergami, R. Alaggio, B. Briseghella, and M. Fragiacomo,

 https://doi.org/10.52202/069179-0411

Effect of pinching on structural resilience: performance of reinforced concrete and timber structures under repeated cycles, *Struct. Infrastruct. Eng.*, pp. 1–17, 2022.

[33] W. Y. Loo, P. Quenneville, and N. Chouw, A numerical study of the seismic behaviour of timber shear walls with slip-friction connectors, *Eng. Struct.*, vol. 34, pp. 233–243, 2012, doi: https://doi.org/10.1016/j.engstruct.2011.09.016.

[34] W. Y. Loo, P. Quenneville, and N. Chouw, Rocking Timber Structure with Slip-Friction Connectors Conceptualized As a Plastically Deformable Hinge within a Multistory Shear Wall, *J. Struct. Eng.*, vol. 142, no. 4, p. E4015010, 2016, doi: 10.1061/(ASCE)ST.1943-541X.0001387.

[35] D. Fitzgerald, T. H. Miller, A. Sinha, and J. A. Nairn, Cross-laminated timber rocking walls with slip-friction connections, *Eng. Struct.*, vol. 220, p. 110973, 2020.

[36] A. Hashemi, P. Zarnani, R. Masoudnia, and P. Quenneville, Experimental testing of rocking cross-laminated timber walls with resilient slip friction joints, *J. Struct. Eng.*, vol. 144, no. 1, p. 4017180, 2018.

[37] A. Aloisio, M. Pelliciari, S. Sirotti, F. Boggian, and R. Tomasi, Optimization of the structural coupling between RC frames, CLT shear walls and asymmetric friction connections, *Bull. Earthq. Eng.*, pp. 1–26, 2022.

[38] F. Boggian, C. Tardo, A. Aloisio, E. M. Marino, and R. Tomasi, Experimental cyclic response of a novel friction connection for seismic retrofitting of RC buildings with CLT panels, *J. Struct. Eng.*, vol. In press, 2022, doi: 10.1061/(ASCE)ST.1943-541X.0003313.

[39] A. Aloisio, F. Boggian, and R. Tomasi, Design of a novel seismic retrofitting system for RC structures based on asymmetric friction connections and CLT panels, *Eng. Struct.*, vol. 254, p. 113807, 2022.

[40] P. Gardoni, A. Der Kiureghian, and K. M. Mosalam, Probabilistic capacity models and fragility estimates for reinforced concrete columns based on experimental observations, *J. Eng. Mech.*, vol. 128, no. 10, pp. 1024–1038, 2002.